NASA TECHNICAL NOTE

NASA TN D-4852

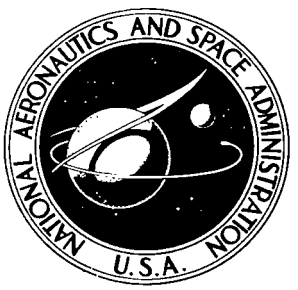

NASA TN D-4852

PLANETARY PROBE GUIDANCE ACCURACY INFLUENCE FACTORS FOR CONJUNCTION-CLASS MISSIONS

by Thomas B. Murtagh

Manned Spacecraft Center
Houston, Texas

NATIONAL AERONAUTICS AND SPACE ADMINISTRATION • WASHINGTON, D. C. • JANUARY 1969

NASA TN D-4852

PLANETARY PROBE GUIDANCE ACCURACY INFLUENCE FACTORS FOR CONJUNCTION-CLASS MISSIONS

By Thomas B. Murtagh

Manned Spacecraft Center
Houston, Texas

NATIONAL AERONAUTICS AND SPACE ADMINISTRATION

For sale by the Clearinghouse for Federal Scientific and Technical Information
Springfield, Virginia 22151 – CFSTI price $3.00

ABSTRACT

The influence of spacecraft onboard-radar data type and accuracy, of nominal entry trajectory parameters, and of planet radius uncertainty for unmanned planetary probe guidance is presented for a typical conjunction-class mission. The results of the analysis indicate that a probe guidance corridor on the order of 24 nautical miles can be obtained for a total midcourse velocity requirement less than 100 fps. The corridor results were more sensitive to variations in the nominal entry trajectory parameters than to variations in the assumed error in the radius of the target planet.

CONTENTS

TABLES

FIGURES

PLANETARY PROBE GUIDANCE ACCURACY INFLUENCE FACTORS FOR CONJUNCTION-CLASS MISSIONS

By Thomas B. Murtagh
Manned Spacecraft Center

SUMMARY

The influence of spacecraft onboard-radar data type and accuracy, of nominal entry trajectory parameters, and of planet radius uncertainty for unmanned planetary probe guidance is presented for a typical conjunction-class mission. The probe is assumed to be deployed from a manned spacecraft at the target-planet sphere of influence, with the inclination of the probe trajectory equal to the inclination of the spacecraft approach hyperbola. The results of the analysis indicate that a probe vacuum periapsis-radius error on the order of 4 nautical miles (guidance corridor equal to 24 nautical miles) can be obtained for a total midcourse velocity requirement less than 100 fps. The corridor results were more sensitive to variations in the nominal entry trajectory parameters than to variations in the assumed error in the radius of the target planet.

INTRODUCTION

The analysis in this report represents an extension of the analysis presented in reference 1, and some of the assumptions contained in reference 1 are investigated in more detail. The most significant assumption proposed in that report was the hypothesis that the radar on board the manned spacecraft could precisely measure the relative range and/or range-rate to the unmanned probe. This means, in effect, that the state-vector estimates for the probe and spacecraft have equivalent accuracy. In reference 1, the nominal probe entry trajectory was constrained in such a manner that the probe would arrive at the nominal entry altitude approximately 1 hour prior to the spacecraft arrival at the periapsis of the approach hyperbola. These nominal entry parameters were fixed in order to simplify the analysis presented in the report. The entry parameters are, however, a function of the type of probe mission considered. For example, shallow entry flight-path angles are desired for probe missions that require a "skip" out of the atmosphere into an orbit about the planet; impact-type probes require much steeper flight-path angles. For the analysis presented in this report, a reference probe mission was arbitrarily chosen in order to determine the effect of spacecraft onboard-radar data type (range and/or range-rate) and accuracy on the entry guidance corridor. Variations in planet radius error and in nominal entry trajectory parameters were also considered in order to illustrate their influence on the entry corridor.

In the first section of this report, the assumptions made in the analysis are discussed, followed by a section concerned with the reference mission used in the analysis. The spacecraft/probe navigation- and guidance-system configurations are then outlined, followed by the section entitled "Results and Discussion."

The author wishes to thank George P. Callas of the NASA Ames Research Center for his comments on the mathematical development presented in this report.

SYMBOLS

A	sensitivity vector that relates star/planet-horizon included-angle deviations to spacecraft state-vector deviations
B	sensitivity matrix that relates spacecraft/probe relative range/range-rate deviations to spacecraft/probe state-vector deviations
C	6×3 compatibility matrix defined by $\begin{pmatrix} 0 \\ I \end{pmatrix}$
E_p	6×6 probe uncertainty covariance matrix
E_s	6×6 spacecraft uncertainty covariance matrix
G	6×6 guidance matrix
G_1, G_2	3×3 submatrices of the guidance matrix
H	3×12 sensitivity matrix defined by equation (9)
I	identity matrix of appropriate dimensions
K	12×3 weighting matrix defined by equation (13)
L	3×3 matrix defined by equation (16)
M	3×3 matrix defined by equation (13)
N	3×3 covariance matrix of velocity-correction execution error
P	12×12 uncertainty covariance matrix for the coupled spacecraft/probe system
P_i	submatrices of the uncertainty covariance matrix, $i = 1, \ldots, 4$
R	3×3 covariance matrix of measurement errors, defined by equation (14)

r_B	planet radius
$\vec{r}_p$	probe position vector with respect to the target planet
r_s	magnitude of the spacecraft position vector
$\vec{r}_s$	spacecraft position vector with respect to the target planet
$\hat{r}_{star}$	unit vector to a star
t	current time
t_0	time of spacecraft/probe separation
$\vec{V}_p$	probe velocity vector with respect to the target planet
$\vec{V}_s$	spacecraft velocity vector with respect to the target planet
$\vec{V}_\rho$	spacecraft/probe relative velocity vector, $\vec{V}_\rho = \vec{V}_p - \vec{V}_s$
X_p	6×6 probe dispersion covariance matrix
X_s	6×6 spacecraft dispersion covariance matrix
β	star/planet-horizon included angle
$\Gamma(\tau, t)$	6×6 probe state transition matrix
γ_e	entry flight-path angle
ΔE	degradation to $E_p(\tau)$ as a result of the spacecraft/probe separation maneuver
$\delta( )$	small deviation from the reference value
$\vec{\xi}$	12-dimensional augmented state vector
$\Theta(\tau, t)$	12×12 augmented state transition matrix defined by equation (3)

θ	one-half the planet disk subtended angle, $\sin\theta = r_B/r_s$
ρ	magnitude of the probe relative position vector
$\vec{\rho}$	probe relative position vector with respect to the spacecraft, $\vec{\rho} = \vec{r}_p - \vec{r}_s$
$\dot{\rho}$	spacecraft/probe relative range-rate, $\dot{\rho} = \frac{\vec{\rho}}{\rho} \cdot \vec{V}_\rho$
σ_β^2	variance of star/planet-horizon observable
σ_ρ^2	onboard-radar range variance
$\sigma_{\dot{\rho}}^2$	onboard-radar range-rate variance
τ	projected time
$\Phi(\tau, t)$	6×6 spacecraft state transition matrix

Subscripts:

max	maximum
sep	separation

Superscripts:

-1	inverse
T	transpose
+	after navigation measurement or guidance maneuver
-	before navigation measurement or guidance maneuver

ANALYSIS

Assumptions

The following ground rules are postulated for the analysis.

1. The unmanned probe is deployed from the manned spacecraft at the target-planet sphere of influence (SOI), with the inclination of the probe trajectory equal to the inclination of the spacecraft approach hyperbola.

2. Spacecraft and probe position and velocity uncertainties are reduced by simultaneously processing both onboard-radar relative range and/or range-rate data from the spacecraft to the probe and star/planet-horizon included-angle data from the spacecraft, using a Kalman filter.

3. Conic reference trajectories are assumed, and the state transition matrix used to propagate the errors is derived analytically for two-body conic trajectories.

4. Variable-time-of-arrival (VTA) guidance logic is used to compute the root-mean-square (rms) velocity corrections for the probe and to compute the corresponding vacuum periapsis-radius dispersions. Variable-time-of-arrival guidance logic constrains the radial and cross-range components of the vehicle position at a terminal time slightly different from the nominal time, while minimizing the magnitude of the commanded correction (ref. 1). The entry guidance corridor is computed by multiplying the radius dispersion by a factor of 6 ($\pm 3\sigma$ about the nominal).

5. A summary of the assumed navigation- and guidance-system nominal errors is presented in table I. With the exception of the Mars radius error, measurement and dynamic biases are not considered in order to simplify the analysis.

Reference Mission

A typical conjunction-class mission was chosen for the analysis presented in this report. This reference mission was a 1977 Mars stopover mission with a 360-day outbound trip, a 300-day Mars orbit, and a 320-day return to Earth (ref. 2). The reference trajectory characteristics for this mission are summarized in table II.

The Earth-injection covariance matrix for the reference trajectory was diagonal, with rms position and velocity errors of 4 nautical miles and 16 fps, respectively. Earth-based-radar range and range-rate data were processed during the departure phase of the mission (i.e., within the Earth SOI), with onboard-sextant planet-star tracking in the heliocentric phase (i.e., between the Earth and Mars SOI). For the onboard measurements, the sighting body was selected according to the optimality criterion outlined in reference 3. The error model assumed for the Earth-based radar system is discussed in reference 4, and the onboard-sextant error model is presented in reference 1.

The Earth-based-radar and onboard optical navigation data were processed every 30 minutes and each half-day during the departure and heliocentric phases, respectively. Three midcourse fixed-time-of-arrival (FTA) velocity corrections requiring a total ΔV of 74 fps were executed to update the spacecraft dispersion matrix prior to the unmanned-probe deployment at the Mars SOI (approximately 312 000 nautical miles from Mars).

Spacecraft/Probe Navigation and Guidance Systems

The spacecraft/probe tracking geometry is illustrated in figure 1. For this analysis, it was assumed that the spacecraft onboard radar could measure the relative range and/or range-rate to the probe and simultaneously use an onboard optical sensor (i.e., sextant) to measure the included angle between the Mars horizon and a star. This procedure seems feasible since the onboard radar can track the probe continuously and since, when the spacecraft horizon-star measurement is fed into the onboard computer, a command that would call for simultaneous data processing of the radar range and/or range-rate information could automatically be set up in the navigation program.

The navigation data can be processed in the onboard computer using a Kalman filter. The structure of the filter equations for the coupled spacecraft/probe system is identical to the conventional Kalman equations, but with increased state-vector dimensions (refs. 5 and 6). For the problem considered in this report, the state vector is 12-dimensional and includes spacecraft position and velocity, as well as unmanned-probe position and velocity. The equation which relates deviations in this state vector at time τ to deviations at time t is

$$\begin{bmatrix} \delta\vec{r}_s(\tau) \\ \delta\vec{V}_s(\tau) \\ \delta\vec{r}_p(\tau) \\ \delta\vec{V}_p(\tau) \end{bmatrix} = \begin{bmatrix} \Phi(\tau, t) & 0 \\ 0 & \Gamma(\tau, t) \end{bmatrix} \begin{bmatrix} \delta\vec{r}_s(t) \\ \delta\vec{V}_s(t) \\ \delta\vec{r}_p(t) \\ \delta\vec{V}_p(t) \end{bmatrix} \tag{1}$$

where $\Phi(\tau, t)$ and $\Gamma(\tau, t)$ are the spacecraft and probe state transition matrices, respectively. If

$$\delta\vec{\xi}(\tau) = \begin{bmatrix} \delta\vec{r}_s(\tau) \\ \delta\vec{V}_s(\tau) \\ \delta\vec{r}_p(\tau) \\ \delta\vec{V}_p(\tau) \end{bmatrix} \tag{2}$$

and

$$\Theta(\tau, t) = \begin{bmatrix} \Phi(\tau, t) & 0 \\ 0 & \Gamma(\tau, t) \end{bmatrix} \tag{3}$$

then equation (1) becomes

$$\delta\vec{\xi}(\tau) = \Theta(\tau, t)\delta\vec{\xi}(t) \tag{4}$$

The initial covariance matrix for the coupled system (i.e., at spacecraft/probe separation) is

$$P(t_0) = \begin{bmatrix} E_s(t_0) & E_s(t_0) \\ E_s(t_0) & E_p(t_0) \end{bmatrix} \tag{5}$$

where $E_s(t_0)$ is the spacecraft uncertainty covariance matrix and

$$E_p(t_0) = E_s(t_0) + \Delta E(t_0) \tag{6}$$

The term $\Delta E(t_0)$ is the degradation to the probe uncertainty matrix as a result of the assumed imperfect separation maneuver. The equation for propagating the augmented

uncertainty matrix between measurements is

$$P(\tau) = \Theta(\tau, t)P(t)\Theta^{T}(\tau, t) \tag{7}$$

The equation which relates deviations in the observables (i. e., star-horizon angle, range, range-rate) to state-vector deviations is

$$\begin{bmatrix} \delta\beta(\tau) \\ \delta\rho(\tau) \\ \delta\dot{\rho}(\tau) \end{bmatrix} = H(\tau)\delta\vec{\zeta}(\tau) \tag{8}$$

where the matrix $H(\tau)$ is written in partitioned form as

$$H(\tau) = \begin{bmatrix} A(\tau) & 0 \\ -B(\tau) & B(\tau) \end{bmatrix} \tag{9}$$

The vector $A(\tau)$ is defined by

$$A(\tau) = \begin{bmatrix} \dfrac{\partial\beta}{\partial\vec{r}_s} & \dfrac{\partial\beta}{\partial\vec{V}_s} \end{bmatrix} \tag{10}$$

and the 2×6 matrix $B(\tau)$ is given by

$$B(\tau) = \begin{bmatrix} \dfrac{\partial\rho}{\partial\vec{\rho}} & \dfrac{\partial\rho}{\partial\vec{V}_\rho} \\ \dfrac{\partial\dot{\rho}}{\partial\vec{\rho}} & \dfrac{\partial\dot{\rho}}{\partial\vec{V}_\rho} \end{bmatrix} \tag{11}$$

The partial derivatives required in equations (10) and (11) can be computed from the following relationships (fig. 1).

$$\left.\begin{aligned} \frac{\partial \beta}{\partial \vec{r}_s} &= \frac{r_B}{r_s^3 \cos\theta}\vec{r}_s + \frac{\vec{r}_s \times \left(\vec{r}_s \times \hat{r}_{star}\right)}{r_s^2 \left|\vec{r}_s \times \hat{r}_{star}\right|} \\ \frac{\partial \beta}{\partial \vec{V}_s} &= 0 \end{aligned}\right\} \qquad (12a)$$

$$\left.\begin{aligned} \frac{\partial \rho}{\partial \vec{\rho}} &= \frac{\vec{\rho}^T}{\rho} \\ \frac{\partial \rho}{\partial \vec{V}_\rho} &= 0 \end{aligned}\right\} \qquad (12b)$$

$$\left.\begin{aligned} \frac{\partial \dot{\rho}}{\partial \vec{\rho}} &= \frac{\vec{V}_\rho^{\,T}}{\rho}\left[I - \frac{\vec{\rho}\vec{\rho}^T}{\rho^2}\right] \\ \frac{\partial \dot{\rho}}{\partial \vec{V}_\rho} &= \frac{\vec{\rho}^T}{\rho} \end{aligned}\right\} \qquad (12c)$$

The equations required in order to update the uncertainty matrix $P(\tau)$ at the time of a measurement can now be written as

$$\left.\begin{aligned} P^+(\tau) &= [I - K(\tau)H(\tau)]P^-(\tau) \\ K(\tau) &= P^-(\tau)H^T(\tau)M^{-1}(\tau) \\ M(\tau) &= H(\tau)P^-(\tau)H^T(\tau) + R(\tau) \end{aligned}\right\} \qquad (13)$$

where the covariance matrix of measurement errors $R(\tau)$ is defined by

$$R(\tau) = \begin{bmatrix} \sigma_\beta^2 & 0 & 0 \\ 0 & \sigma_\rho^2 & 0 \\ 0 & 0 & \sigma_{\dot{\rho}}^2 \end{bmatrix} \tag{14}$$

and the superscripts - and + refer to a quantity before and after the measurement (or correction), respectively.

If it is assumed that the navigation and guidance systems are uncoupled, then the spacecraft and probe dispersion matrices are propagated separately, using the equations

$$\left.\begin{aligned} X_s(\tau) &= \Phi(\tau, t) X_s(t) \Phi^T(\tau, t) \\ X_p(\tau) &= \Gamma(\tau, t) X_p(t) \Gamma^T(\tau, t) \end{aligned}\right\} \tag{15}$$

When reasonable confidence is obtained in the trajectory estimates of either the probe or spacecraft, guidance maneuvers are commanded for the appropriate vehicle to restore the dispersed trajectory to specified nominal conditions. For example, if a guidance correction is commanded for the probe at time τ then the rms estimate of the required ΔV is computed from the square root of the trace of the equation

$$L(\tau) = \left[G_1(\tau) \quad G_2(\tau)\right]\left[X_p(\tau) - P_4(\tau)\right]\left[G_1(\tau) \quad G_2(\tau)\right]^T \tag{16}$$

where $G_1(\tau)$ and $G_2(\tau)$ are submatrices of the guidance matrix $G(\tau)$ discussed in references 1 and 7. The matrix $P_4(\tau)$ is a submatrix of the augmented uncertainty

matrix $P(\tau)$ defined by

$$P(\tau) = \begin{bmatrix} P_1(\tau) & P_2(\tau) \\ P_3(\tau) & P_4(\tau) \end{bmatrix} \tag{17}$$

after one or more navigation measurements are processed. The nonzero matrices $P_2(\tau)$ and $P_3(\tau)$ represent the coupling between the spacecraft and probe state-vector errors.

The probe uncertainty and dispersion matrices are modified according to the following equations (ref. 1).

$$\left.\begin{aligned} P_4^{+}(\tau) &= P_4^{-}(\tau) + CN(\tau)C^T \\ X_p^{+}(\tau) &= [I + G(\tau)]\left[X_p^{-}(\tau) - P_4^{-}(\tau)\right][I + G(\tau)]^T + P_4^{+}(\tau) \end{aligned}\right\} \tag{18}$$

Equations similar to (16) and (18) are used to calculate the rms ΔV and matrix updates for the spacecraft if $X_p(\tau)$ and $P_4(\tau)$ are replaced by $X_s(\tau)$ and $P_1(\tau)$, respectively. The covariance matrix of velocity-correction execution error $N(\tau)$ is derived and discussed in reference 8.

RESULTS AND DISCUSSION

Nominal Probe Trajectory

Assuming that the probe is deployed from the spacecraft at the Mars SOI, with the inclination of the probe trajectory equal to the inclination of the spacecraft approach hyperbola, three entry parameters — altitude, speed, and flight-path angle — remain to be specified. In figure 2, probe separation ΔV is plotted versus the entry parameters. In figure 2(a), variations in entry speed and flight-path angle are considered for an entry altitude of 315 000 feet. The minimum separation velocity occurs when the angle between the separation ΔV vector and the spacecraft velocity vector is approximately 90°. From figure 2(a), it can be seen that the effect on probe separation ΔV of variations in entry flight-path angle becomes more pronounced as the minimum of the curve is approached and decreases rapidly on either side of the minimum. The time required for the probe to reach vacuum periapsis (i. e., the periapsis of the probe trajectory if there were no atmosphere, not shown in fig. 2(a))

is inversely proportional to the entry speed. In figure 2(b), the probe separation ΔV is presented as a function of variation in entry altitude and flight-path angle for a fixed entry speed. From the figure, it is evident that the separation ΔV, for a given flight-path angle, increases almost linearly with increasing entry altitude. For the nominal probe trajectory, an entry altitude of 315 000 feet, an entry speed of 18 350 fps, and an entry flight-path angle of -5° were arbitrarily chosen. Selecting these entry parameter values causes the probe to reach its vacuum periapsis approximately 20 minutes ahead of the spacecraft arrival at the approach-hyperbola periapsis. The separation ΔV required was 45 fps.

In figure 3, the spacecraft/probe relative range is plotted against time from separation for the nominal probe trajectory. This relative range as a function of time is dependent upon the separation ΔV which, in turn, is a function of the specified entry parameters. The nominal probe trajectory chosen is dependent on relative range, since the spacecraft onboard radar must have a maximum range beyond which no tracking is possible. The maximum range to the probe for the nominal probe trajectory was on the order of 2800 nautical miles, so that effective probe tracking could be assumed throughout the probe delivery phase of the mission if the onboard-radar range capability was at least 2800 nautical miles.

Onboard-Radar Data-Type Influence

The effect of spacecraft onboard-radar data type and accuracy on unmanned-probe navigation is illustrated in figure 4. In figure 4(a), it is assumed that the onboard radar processes both range and range-rate data every 30 minutes for three sets of navigation system errors. The profile of the curves in this figure is not entirely what would be expected. The apparent anomaly in the data occurs between 10 and 58 hours from separation. Within this time span, the larger radar errors produce lower projected vacuum periapsis-radius uncertainties than the corresponding smaller radar errors. The explanation for this phenomena is related to the correlation that exists in the uncertainty matrix for the coupled spacecraft/probe system. It should be pointed out that the data weights (i.e., $K(\tau)$) computed by the filter are a function of the spacecraft and the probe uncertainties propagated from a previous measurement. In the region of 10 to 58 hours from separation, the larger radar errors (i.e., σ_ρ = 300 feet and $\sigma_{\dot{\rho}}$ = 3 fps) produce lower projected probe uncertainties than the smaller radar errors (i.e., σ_ρ = 200 feet and $\sigma_{\dot{\rho}}$ = 2 fps). However, the spacecraft errors projected to the approach-hyperbola periapsis (data not shown) during the same time interval are slightly larger for the larger radar errors (i.e., σ_ρ = 300 feet and $\sigma_{\dot{\rho}}$ = 3 fps), compared to values for the smaller radar errors (i.e., σ_ρ = 200 feet and $\sigma_{\dot{\rho}}$ = 2 fps). This implies that the filter, in this time interval, gave slightly more weight to the probe data, compared to the weight given to the simultaneously processed spacecraft data.

In figures 4(b), 4(c), and 4(d), probe navigation data comparing the three possible radar data-type combinations are presented, again assuming that data were processed every 30 minutes. In these figures, the range and range-rate curves were generated by simultaneously processing range and range-rate information in the filter.

The range curve was calculated by processing only range data in the filter in a separate simulation run. A third computer run was required in order to generate the range-rate curve by processing only range-rate data in the filter described by equations (13).

In figure 4(b), between 15 and 57 hours from probe deployment, the range-rate only tracking provided a lower vacuum periapsis-radius uncertainty than the combination of range and range-rate tracking. This effect is caused primarily by the low information content of the range data, which tends to degrade the range and range-rate combination. Had a smaller value of range noise been used, the effect noted would have disappeared, and the range and range-rate tracking data would have produced the smallest vacuum periapsis-radius uncertainty for the entire probe delivery phase.

The lower vacuum periapsis-radius uncertainty is exhibited to a lesser degree in figures 4(c) and 4(d). A possible explanation is that the relative weight of the range-rate data compared to the range data has diminished as the errors were increased.

The probe guidance plots associated with the navigation data in figure 4 are presented in figure 5. Figure 5(a) illustrates the effect of the radar errors on the probe entry guidance corridor when range and range-rate data are processed every 30 minutes. Assume for the moment that a maximum allowable vacuum periapsis-radius dispersion of 4 nautical miles is desired (corridor equal to 24 nautical miles). For the nominal radar errors, an rms midcourse ΔV equal to 80 fps provides this maximum allowable corridor. Increasing the navigation system errors (i. e., $R(\tau)$) by factors of 2 and 3 indicates that the maximum allowable corridor can no longer be obtained.

Figures 5(b), 5(c), and 5(d) illustrate the effect on the guidance corridor of the types of radar tracking for the three sets of radar errors. In these figures, it is obvious that range-rate data alone will not allow the probe to achieve a specified 24-nautical-mile guidance corridor. An examination of figure 3 verifies this result. In this figure, it is evident that the rate of change of the relative range is constant between the time of probe deployment and 55 hours from separation, implying an insensitivity of the range-rate measurement to probe state-vector variations.

Mars Radius Uncertainty Influence

The effect of the Mars radius error on the probe entry guidance corridor is illustrated in figure 6. Nominal navigation system errors are assumed, with range and range-rate measurements processed simultaneously every 30 minutes, using the nominal probe reference trajectory previously discussed. If a guidance corridor of 24 nautical miles is desired (vacuum periapsis-radius dispersion equal to 4 nautical miles), then the midcourse velocity requirements are 40, 80, and 300 fps for Mars radius errors of 2, 10, and 30 nautical miles, respectively.

Nominal Probe Trajectory Influence

The effect of nominal trajectory parameter variation on probe guidance accuracy, using nominal Mars radius and spacecraft onboard-radar errors, is presented in figure 7. Navigation data were processed every 30 minutes.

In figure 7(a), the probe midcourse ΔV is plotted as a function of the rms vacuum periapsis-radius dispersion for three entry-altitude values. The other entry parameters were fixed at their nominal values. As the entry altitude increases, the separation ΔV increases, and the time from separation to vacuum periapsis decreases. It should be pointed out that the maximum relative range between the spacecraft and probe also increases as the entry altitude is increased. Consequently, these guidance results are valid only if the onboard-radar range capability is equal to or greater than 7500 nautical miles. Otherwise, effective probe tracking cannot be assumed throughout delivery of the probe to the entry interface.

Variations in the entry flight-path angle are considered in figure 7(b). As the flight-path angle decreases, the separation ΔV increases slightly, and the time to the probe vacuum periapsis remains almost constant. For a specified corridor, the midcourse ΔV decreases as the flight-path angle is varied from -5° to -40°. These results imply that, for a given tracking-system configuration, impact-type probes can be deployed and targeted for less midcourse ΔV than probes designed to skip out of the atmosphere into orbit about the planet.

Finally, variations in entry speed are illustrated in figure 7(c). Decreasing the entry speed increases the time required for the probe to reach the entry interface and thereby increases the amount of navigation data processed; increasing the entry speed provides the opposite effect.

Spacecraft Navigation and Guidance

All the data discussed in the preceding sections apply to probe navigation and guidance. The spacecraft from which the probe is deployed must also be maneuvered to within some maximum allowable target dispersion. However, in order to keep the length of this report within reason, only a brief sketch of spacecraft data will be presented (fig. 8).

In figure 8(a), the spacecraft navigation data from spacecraft/probe separation to the approximate time of arrival at the approach-hyperbola periapsis are presented. The solid curve represents the projected periapsis-radius uncertainty, assuming that no probe tracking occurs, with Mars horizon-star included-angle measurements processed every 30 minutes. The dashed curve represents similar data, assuming that the spacecraft now tracks the probe. It should be noted that better navigation results are obtained when the spacecraft tracks the probe than when the spacecraft does not track the probe, as a result of the coupling of the spacecraft/probe system through relative range and range-rate measurements. The effect noted is analogous to landmark-location error reduction in orbital navigation problems. In such problems, a spacecraft in orbit about a planet makes optical sightings to poorly defined

landmarks, and the output of the data-processing system produces reductions in the uncertainty associated with landmark position, as well as in the uncertainty associated with the state of the orbiting spacecraft.

The spacecraft guidance results are presented in figure 8(b). Again, an improvement is noted when the spacecraft tracks the probe, as compared to the case when the spacecraft does not track the probe. For example, when a maximum allowable periapsis-radius dispersion of 3 nautical miles is specified, a midcourse ΔV of 13 fps is required if the spacecraft is tracking the probe, compared to a ΔV of 25 fps if no tracking occurs.

The lower values of spacecraft ΔV for a specified periapsis-radius dispersion, compared to the probe results presented in the previous sections, are a result of the fact that the initial spacecraft errors are smaller than the initial probe errors (eq. (6)). If no probe deployment execution errors should occur $\left(\text{i.e.}, \ \Delta E(t_0) = 0\right)$, then the spacecraft and probe guidance results would be approximately the same.

CONCLUDING REMARKS

The influence of spacecraft onboard-radar data type and accuracy, of nominal entry trajectory parameters, and of Mars radius error for unmanned planetary probe guidance has been presented for a typical junction-class mission. The results of the analysis indicate that a probe guidance corridor on the order of 24 nautical miles can be obtained for a total midcourse velocity requirement less than 100 fps. For the cases run, the corridor results were more sensitive to nominal entry trajectory parameter variations than to variations in the assumed Mars radius uncertainty.

Manned Spacecraft Center
National Aeronautics and Space Administration
Houston, Texas, July 5, 1968
981-30-10-00-72

REFERENCES

1. Murtagh, Thomas B.; Lowes, Flora B.; and Bond, Victor R.: Navigation and Guidance Analysis of a Mars Probe Launched From a Manned Flyby Spacecraft. NASA TN D-4512, 1968.

2. Lowes, Flora B.; and Murtagh, Thomas B.: Navigation and Guidance Systems Performance for Three Typical Manned Interplanetary Missions. NASA TN D-4629, 1968.

3. Rohde, Paul J.: The Schedule of Measurements for Analysis of an Onboard Navigation System. NASA CR-71107, 1965.

4. Cicolani, Luigi S.: Interplanetary Midcourse Guidance Using Radar Tracking and Onboard Observation Data. NASA TN D-3623, 1966.

5. Suddath, J. H.; Kidd, R. H. III; and Reinhold, Arnold G.: A Linearized Error Analysis of Onboard Primary Navigation Systems for the Apollo Lunar Module. NASA TN D-4027, 1967.

6. Murtagh, Thomas B.: Analysis of Sextant Navigation Measurements During Lunar Module Rendezvous. NASA TN D-3873, 1967.

7. Cicolani, Luigi S.: Linear Theory of Impulsive Velocity Corrections for Space Mission Guidance. NASA TN D-3365, 1966.

8. White, John S.; Callas, George P.; and Cicolani, Luigi S.: Application of Statistical Filter Theory to the Interplanetary Navigation and Guidance Problem. NASA TN D-2697, 1965.

TABLE I. - NOMINAL 1σ ROOT-MEAN-SQUARE ERROR VALUES

Navigation system:	
Onboard-radar accuracy	
Range, ft	100
Range-rate, fps	1
Onboard-sextant accuracy, sec of arc	10
Mars radius uncertainty, n. mi.	10
Guidance system:	
Proportional, percent	1
Pointing, deg	1
Cut-off, fps	0.5

TABLE II. - REFERENCE 1977 MARS STOPOVER MISSION CHARACTERISTICS

Trajectory designation	Characteristics
Julian date of launch from Earth	2 443 400.0
Earth-injection velocity magnitude, fps	12 652
Outbound trip time, days	360
Mars stopover time, days	300
Return trip time, days	320
Periapsis altitude at Mars, n. mi.	200
General location of Mars approach-hyperbola periapsis (with respect to Mars equator)	Southern Hemisphere
Mars approach-hyperbola periapsis speed, fps	17 800
Entry velocity at Earth, fps	38 463

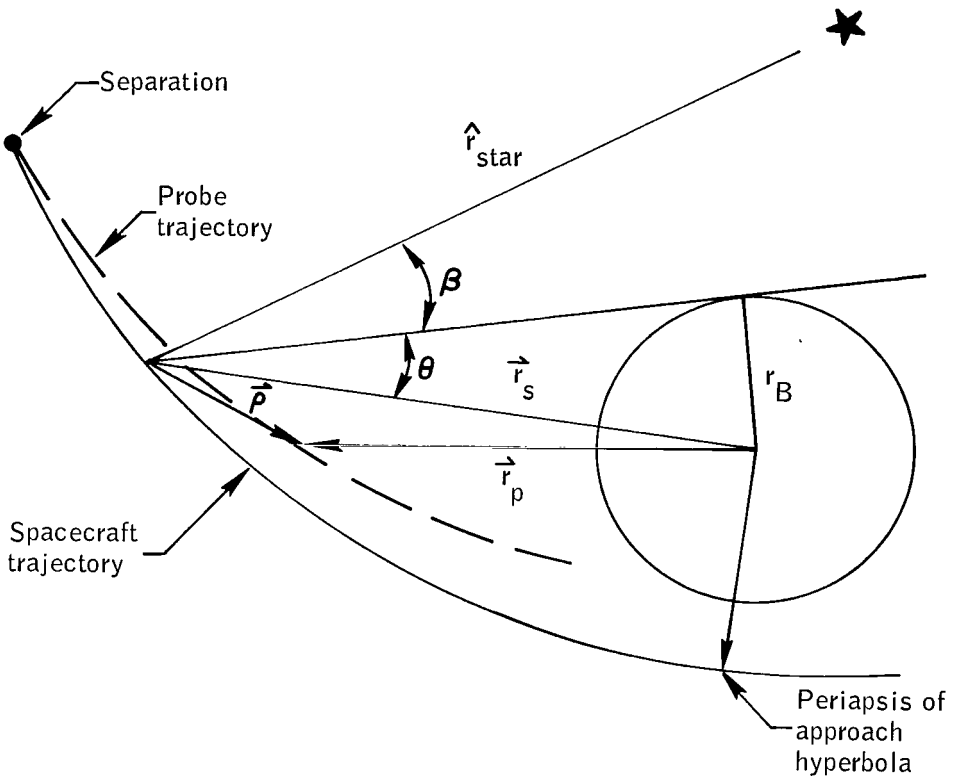

Figure 1. - Spacecraft/probe tracking geometry.

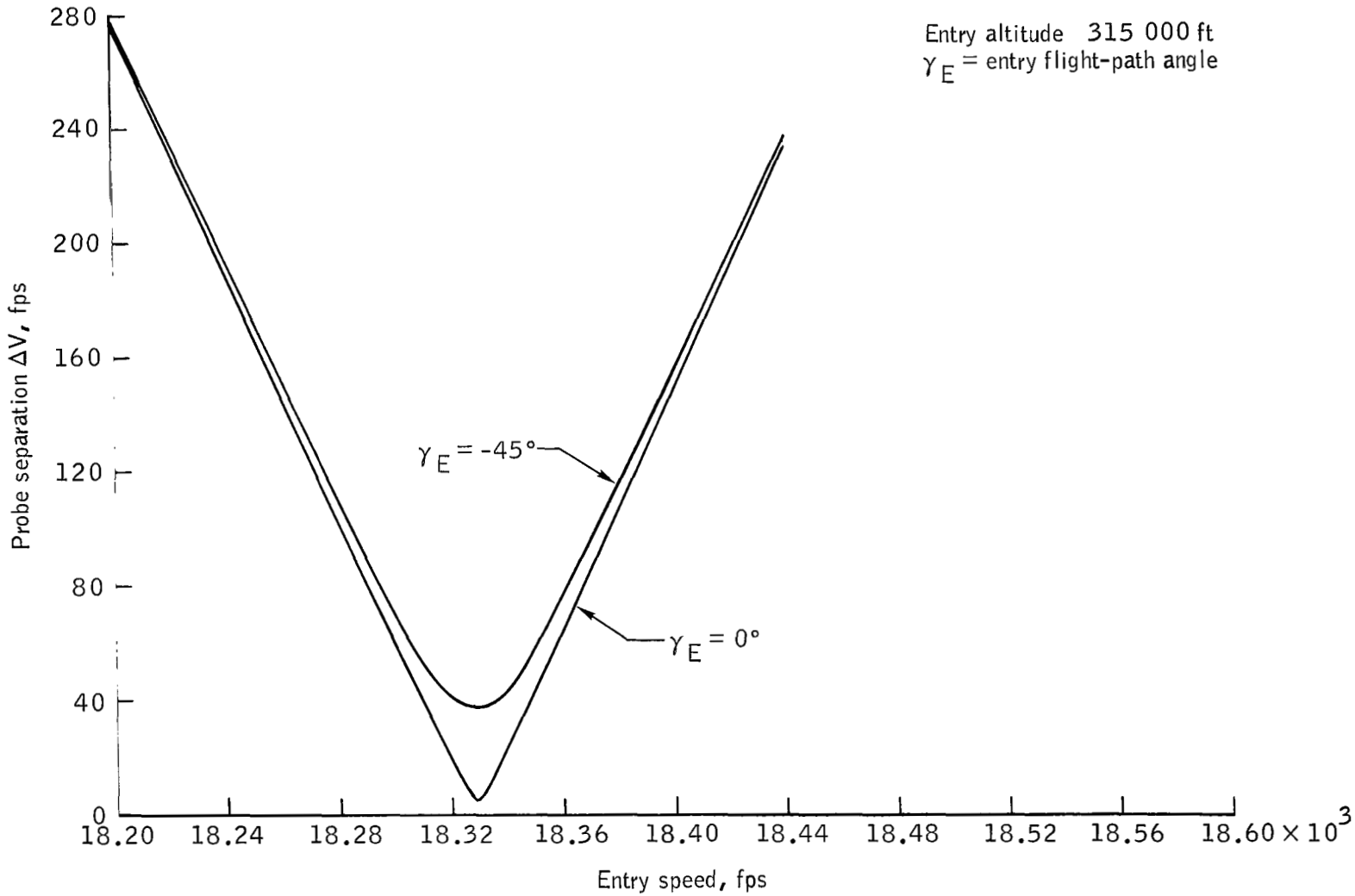

(a) Separation ΔV versus entry speed.

Figure 2. - Probe separation ΔV as a function of entry speed and altitude.

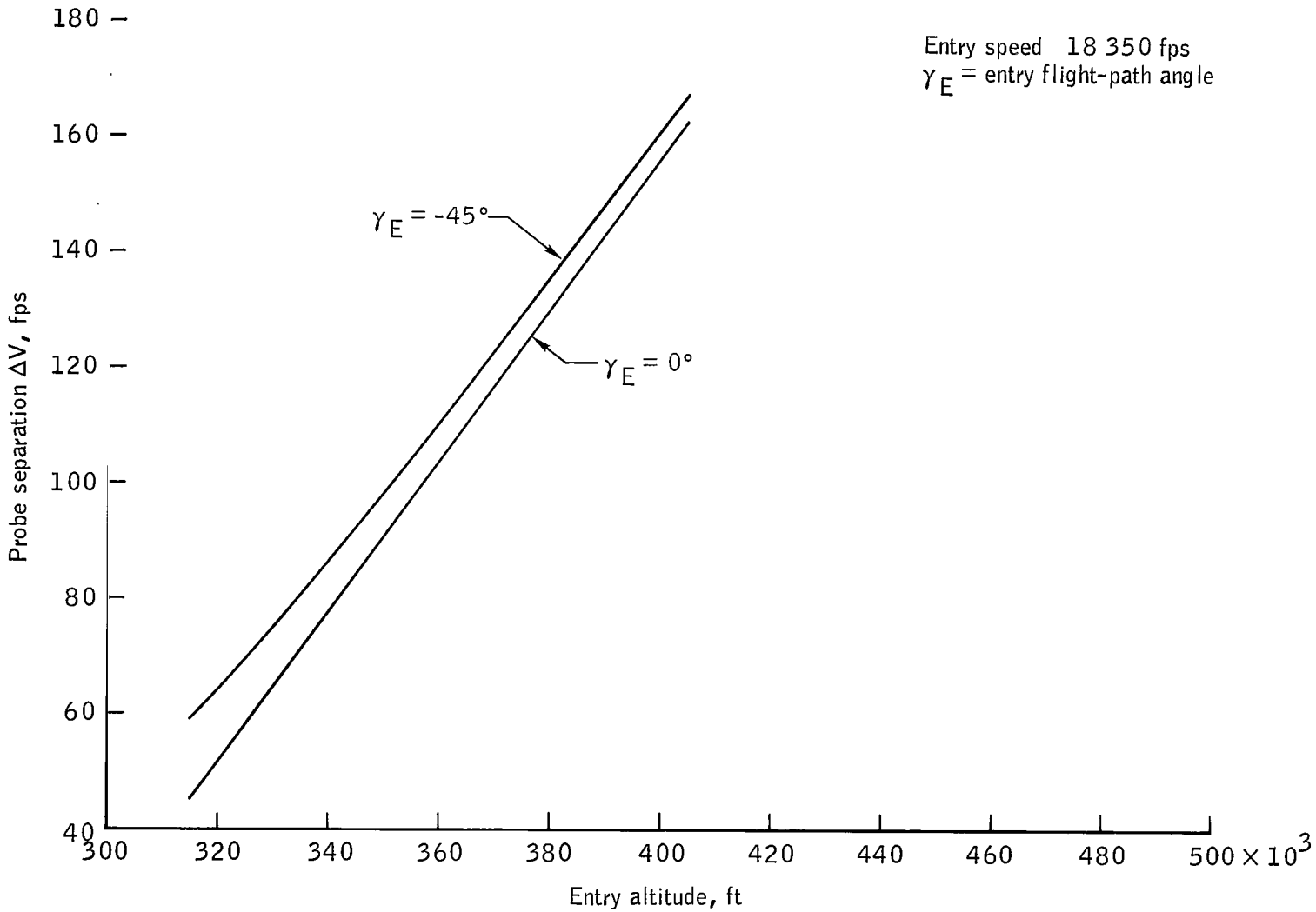

(b) Separation ΔV versus entry altitude.

Figure 2. - Concluded.

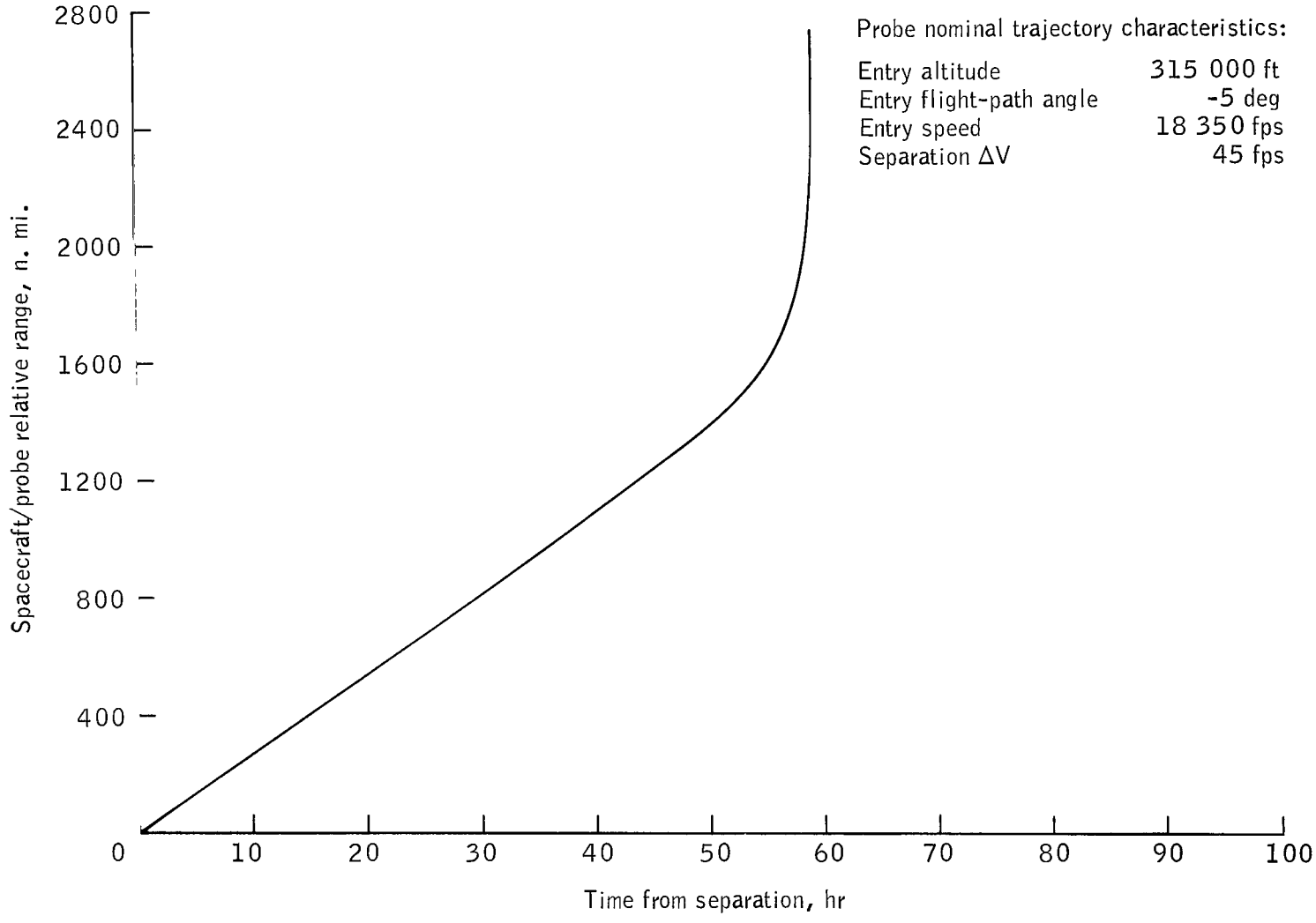

Figure 3. - Spacecraft/probe relative range as a function of time from separation.

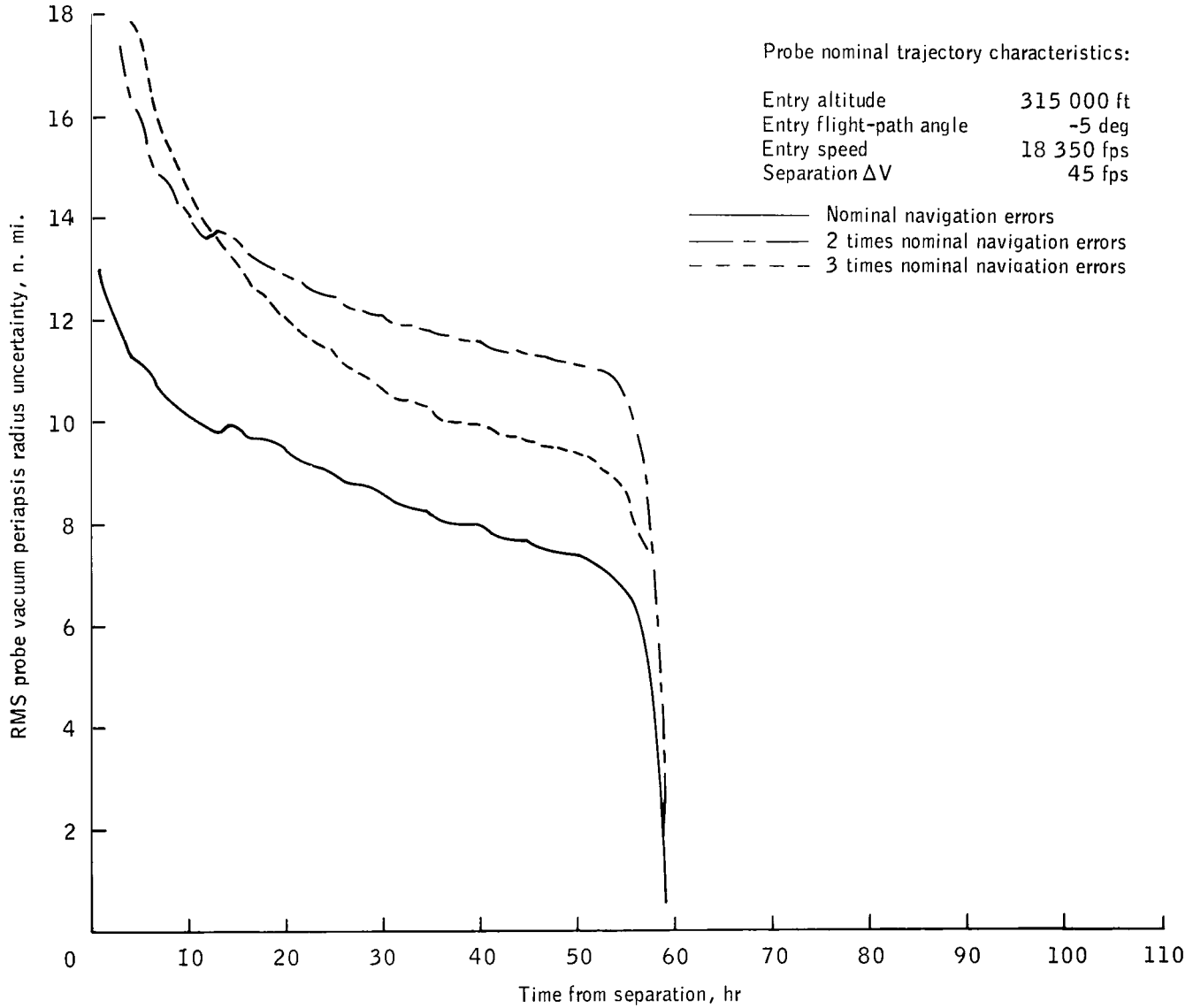

(a) Effect of range/range-rate tracking errors.

Figure 4. - Unmanned-probe anvigation.

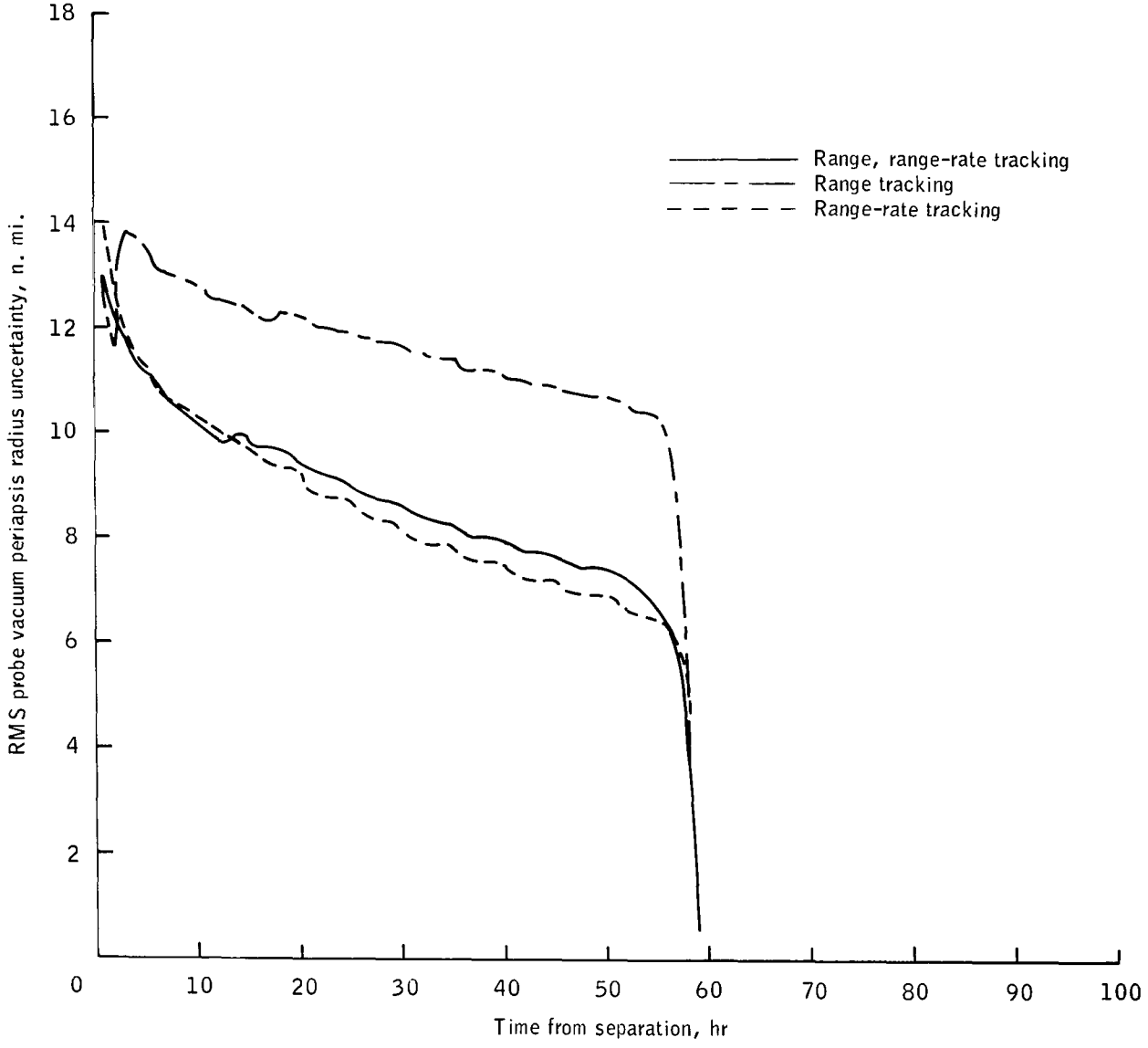

(b) Effect of onboard-radar data type σ_ρ = 100 feet and $\sigma_{\dot{\rho}}$ = 1.0 fps.

Figure 4. - Continued.

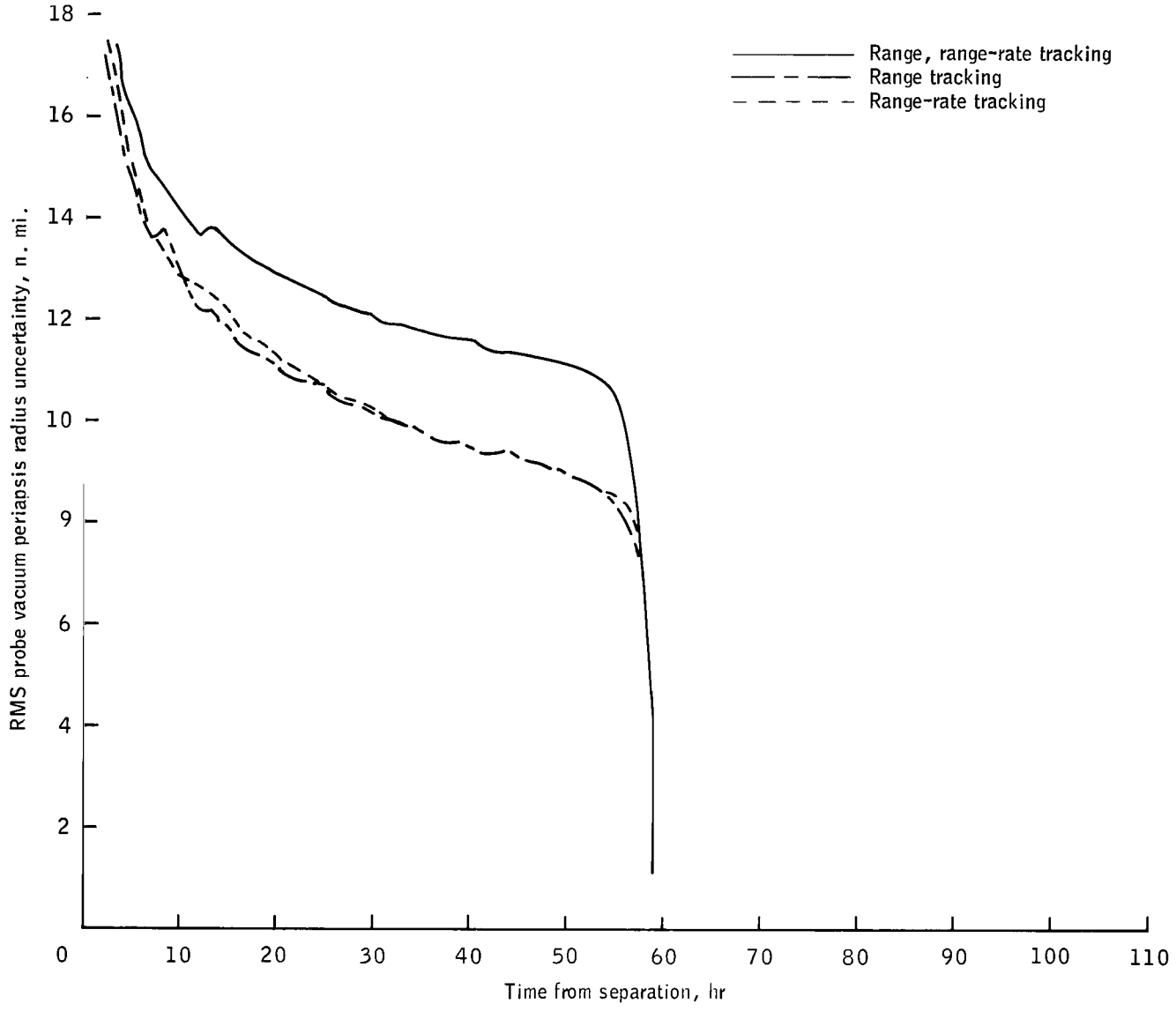

(c) Effect of onboard-radar data type σ_ρ = 200 feet and $\sigma_{\dot{\rho}}$ = 2.0 fps.

Figure 4. - Continued.

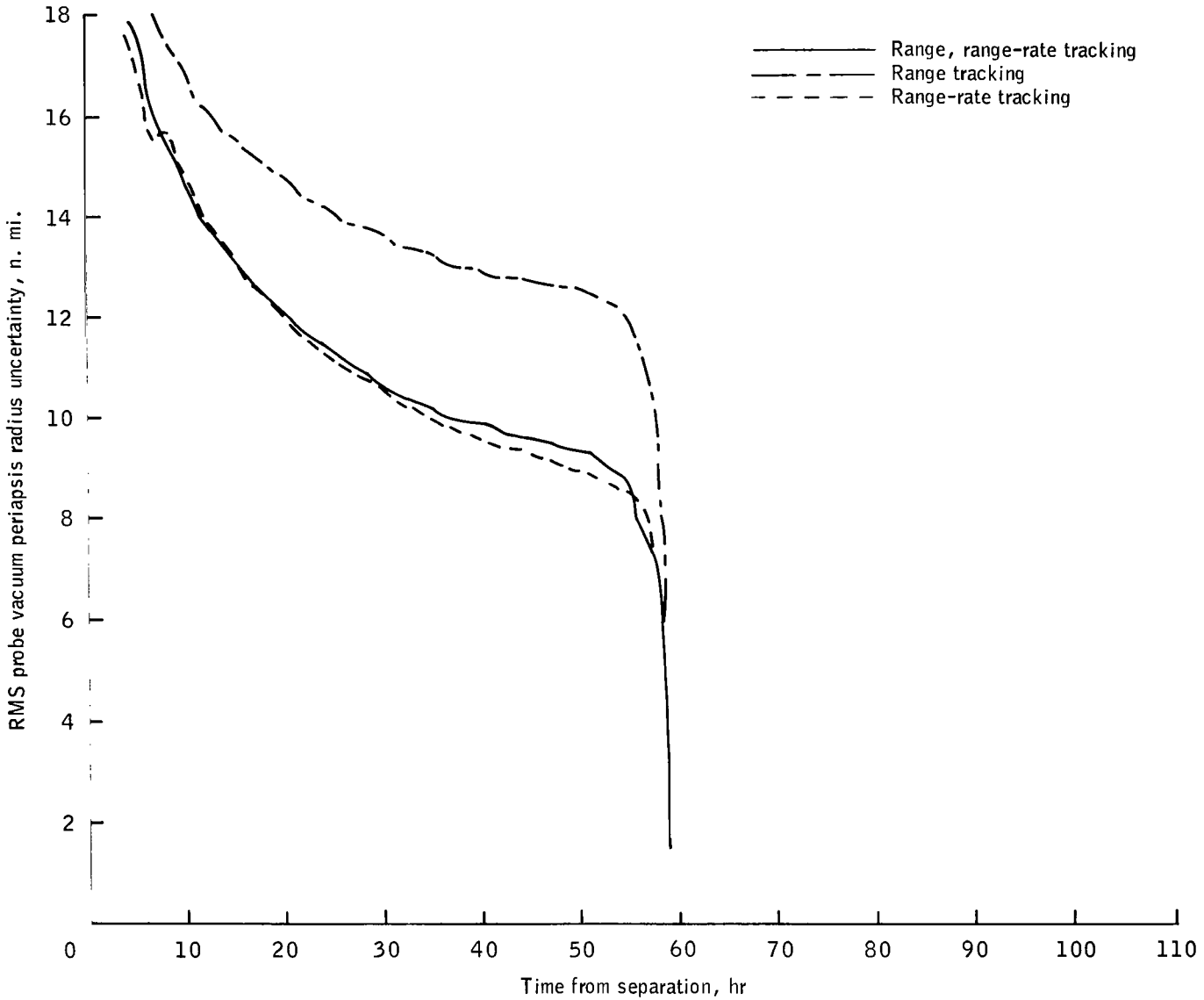

(d) Effect of onboard-radar data type $\sigma_{\rho} = 300$ feet and $\sigma_{\dot{\rho}} = 3.0$ fps.

Figure 4.- Concluded.

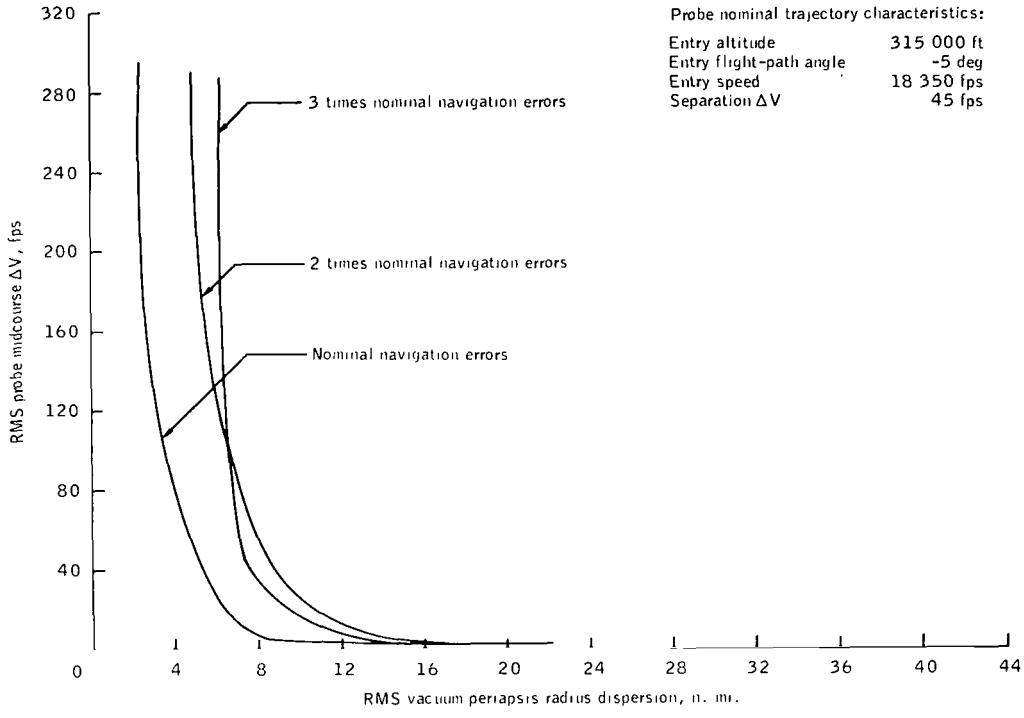

(a) Effect of range/range-rate tracking errors.

Figure 5. - Unmanned-probe guidance.

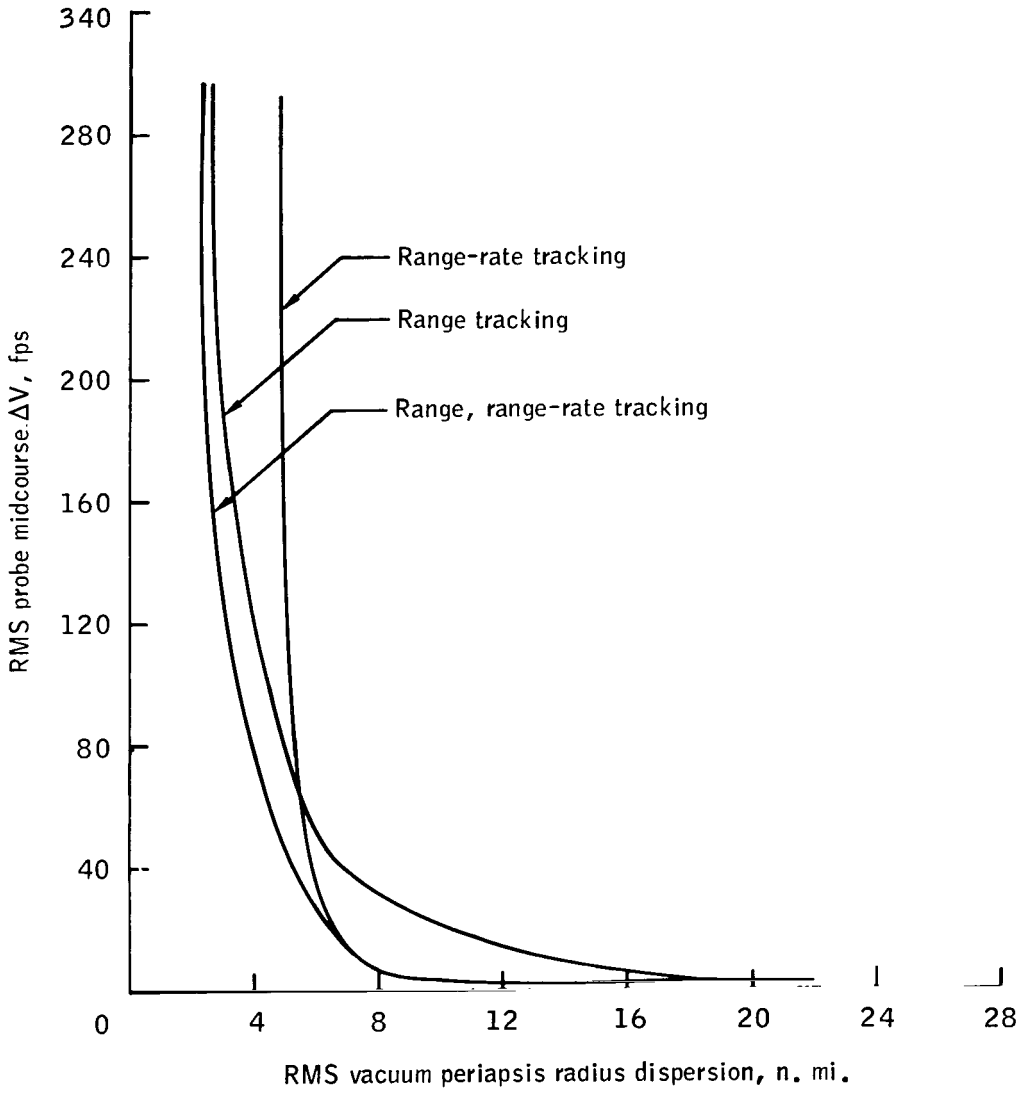

(b) Effect of onboard-radar data type σ_ρ = 100 feet and $\sigma_{\dot{\rho}}$ = 1.0 fps.

Figure 5. - Continued.

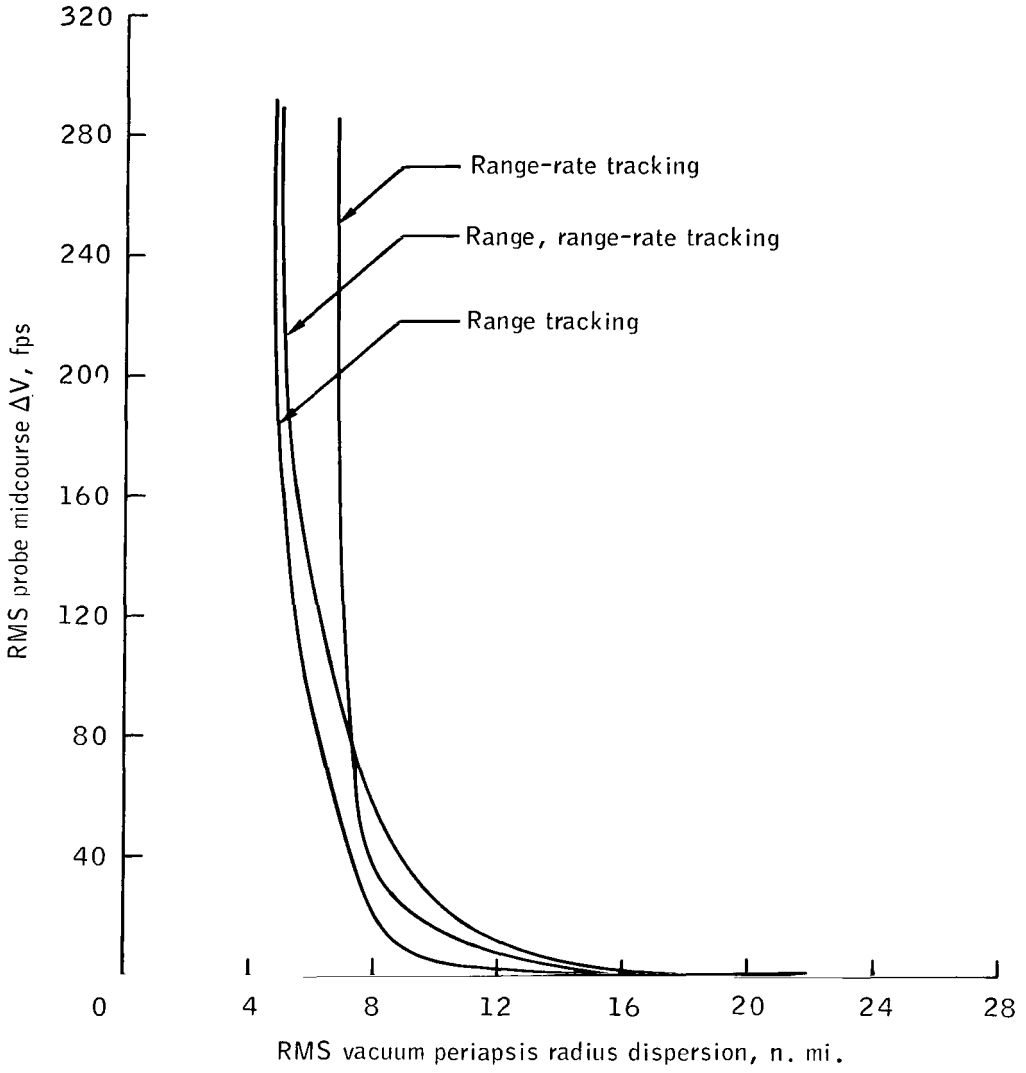

(c) Effect of onboard-radar data type σ_{ρ} = 200 feet and $\sigma_{\dot{\rho}}$ = 2.0 fps.

Figure 5. - Continued.

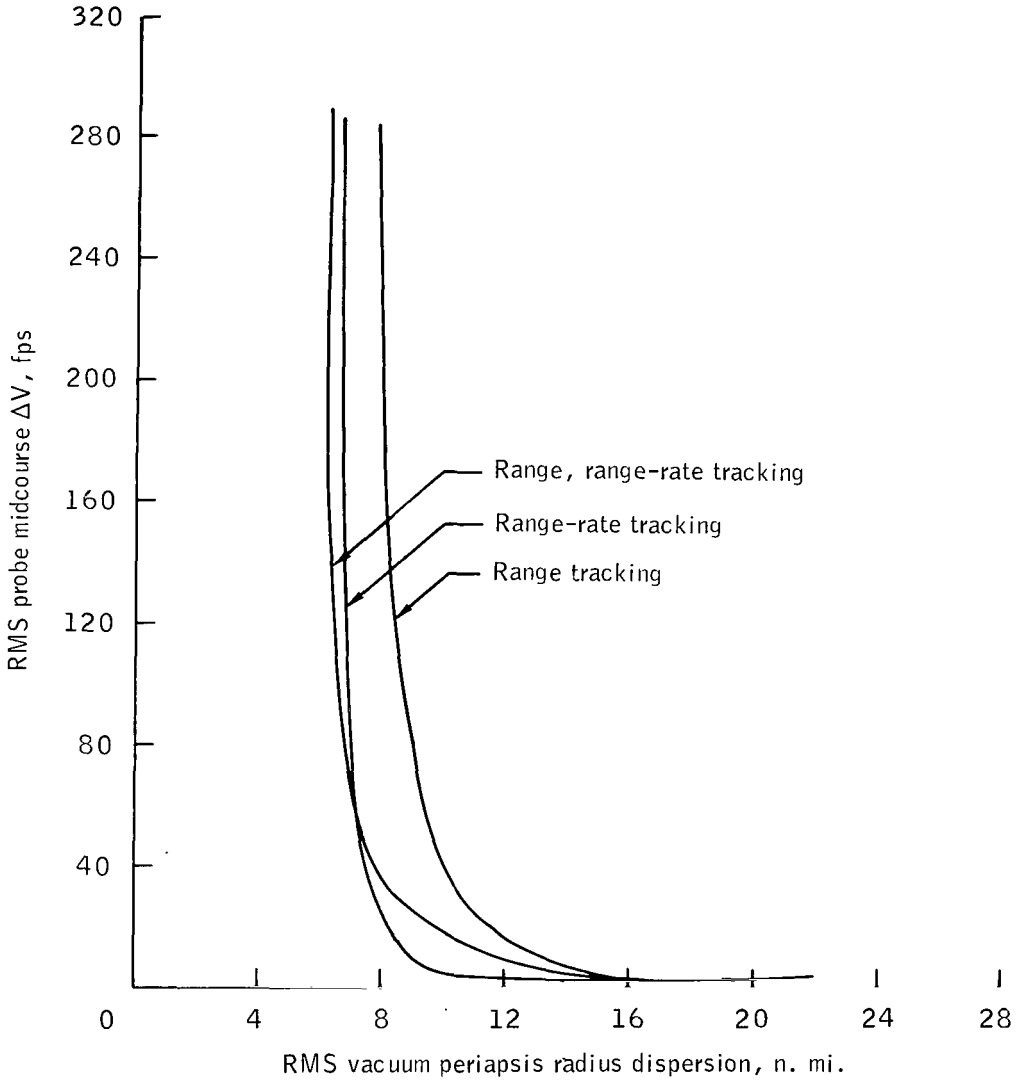

(d) Effect of onboard-radar data type σ_ρ = 300 feet and $\sigma_{\dot{\rho}}$ = 3.0 fps.

Figure 5. - Concluded.

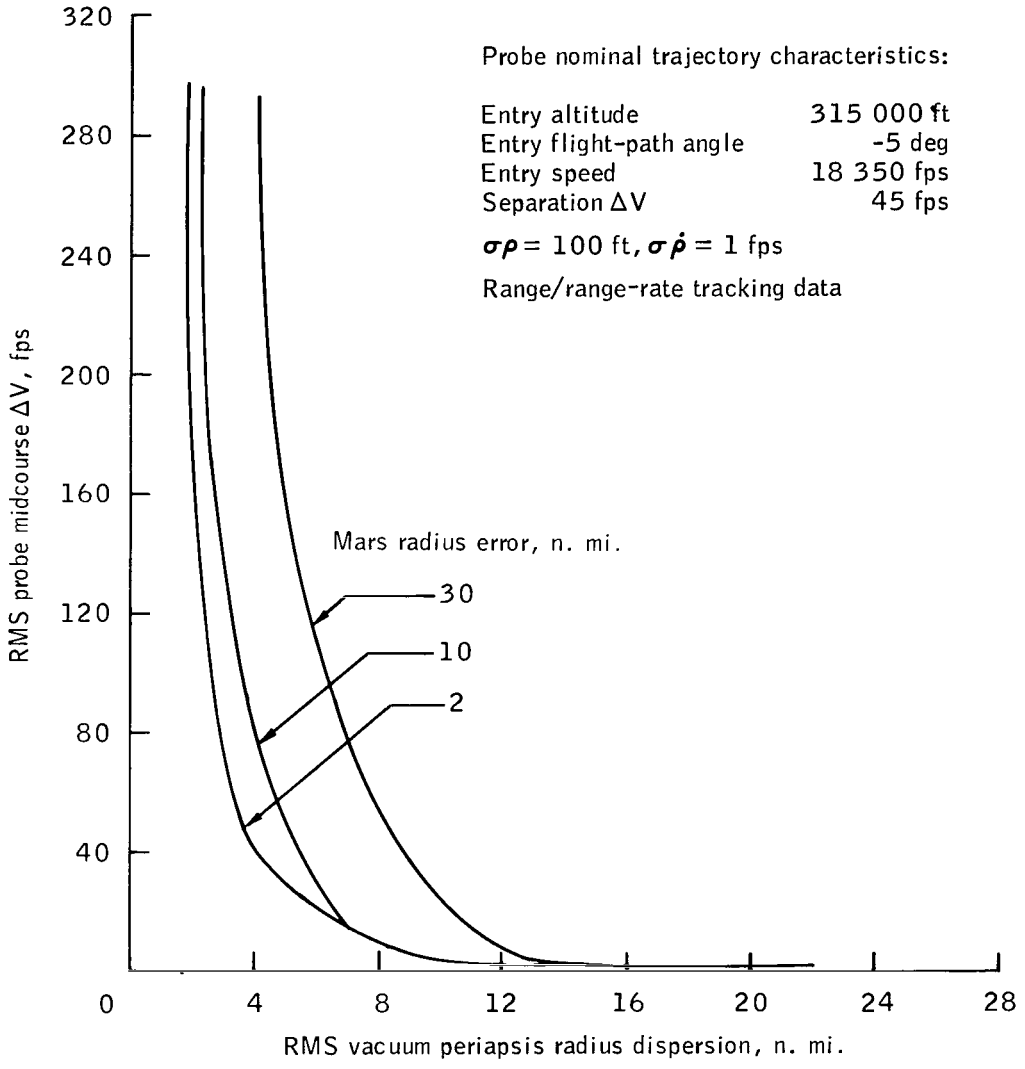

Figure 6.- Effect of Mars radius error on probe guidance.

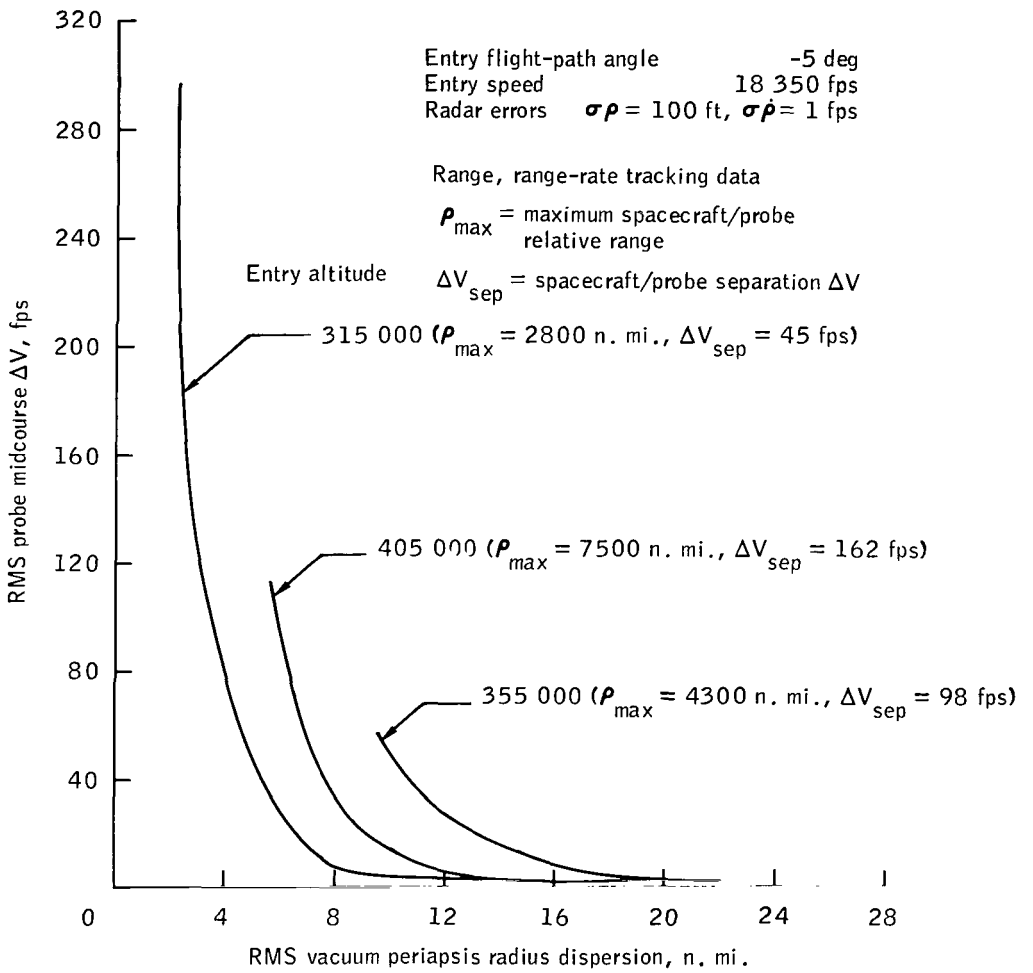

(a) Effect of entry altitude.

Figure 7. - Influence of nominal trajectory parameter variation on probe guidance.

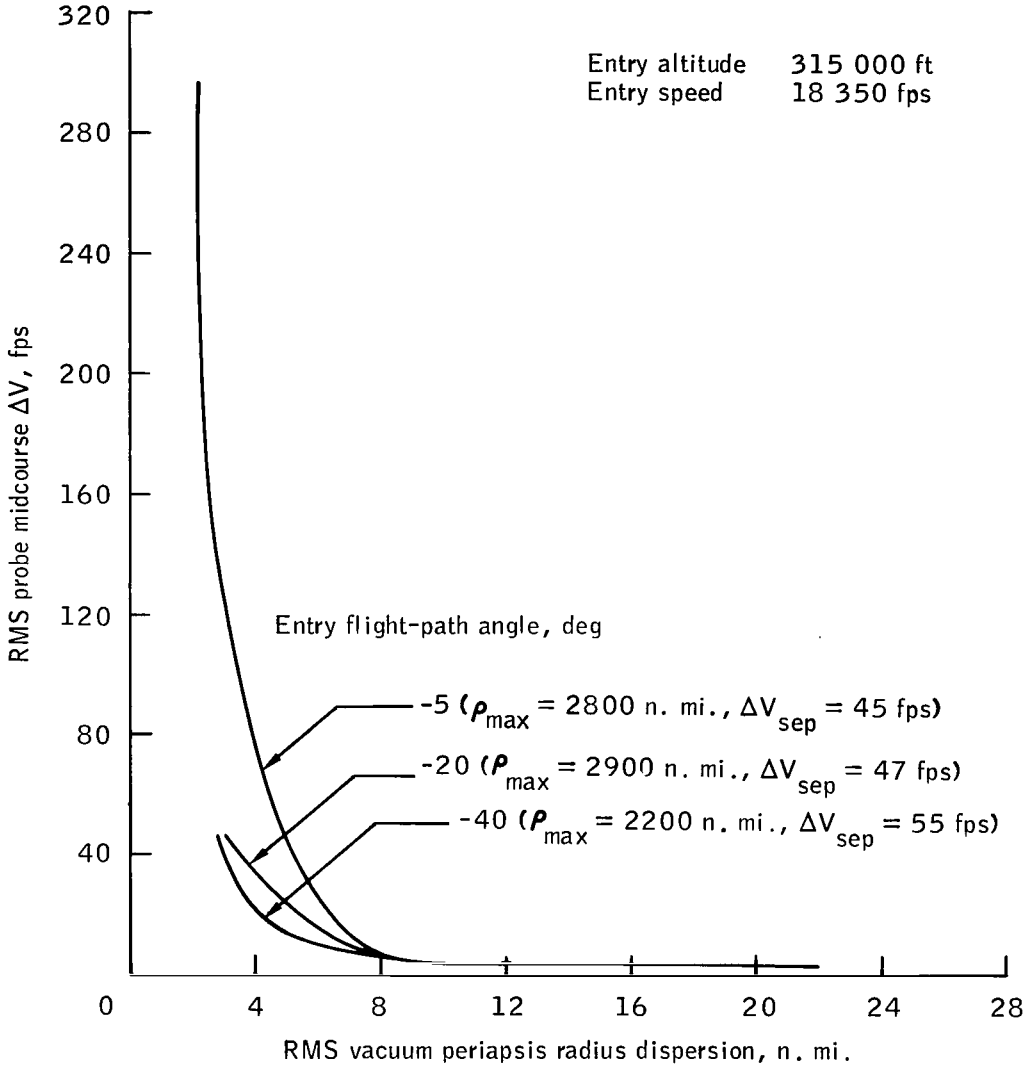

(b) Effect of entry flight-path angle.

Figure 7. - Continued.

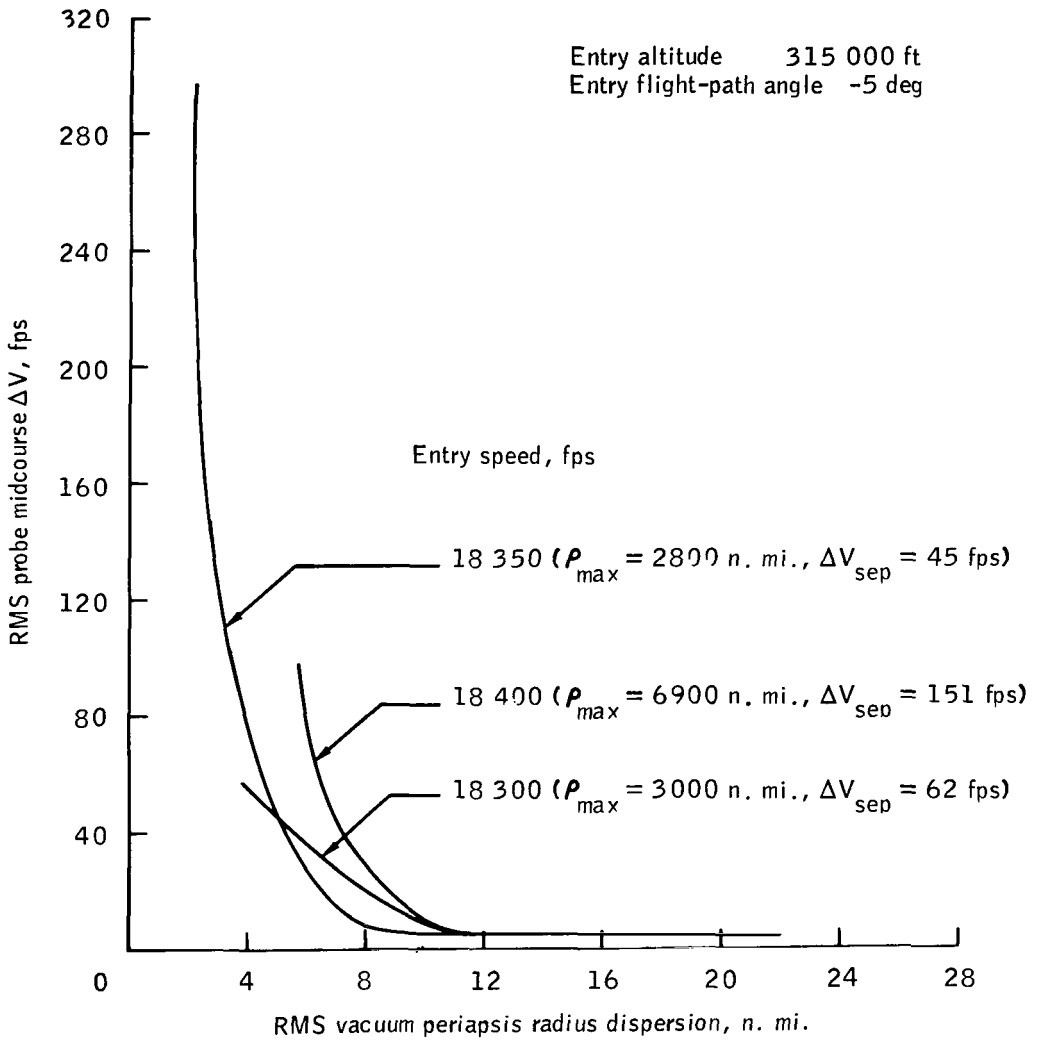

(c) Effect of entry speed.

Figure 7. - Concluded.

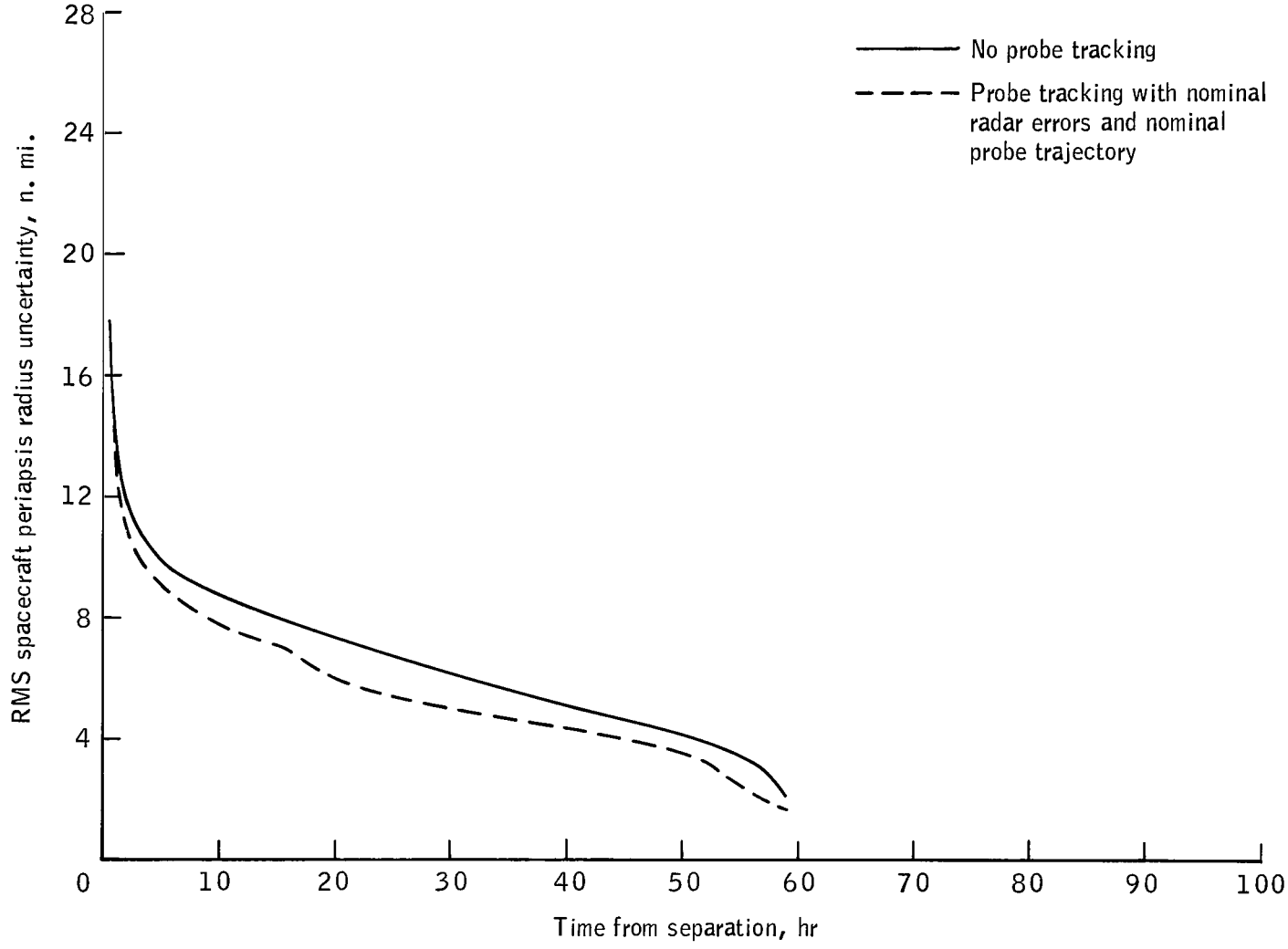

(a) Navigation error.

Figure 8. - Spacecraft errors.

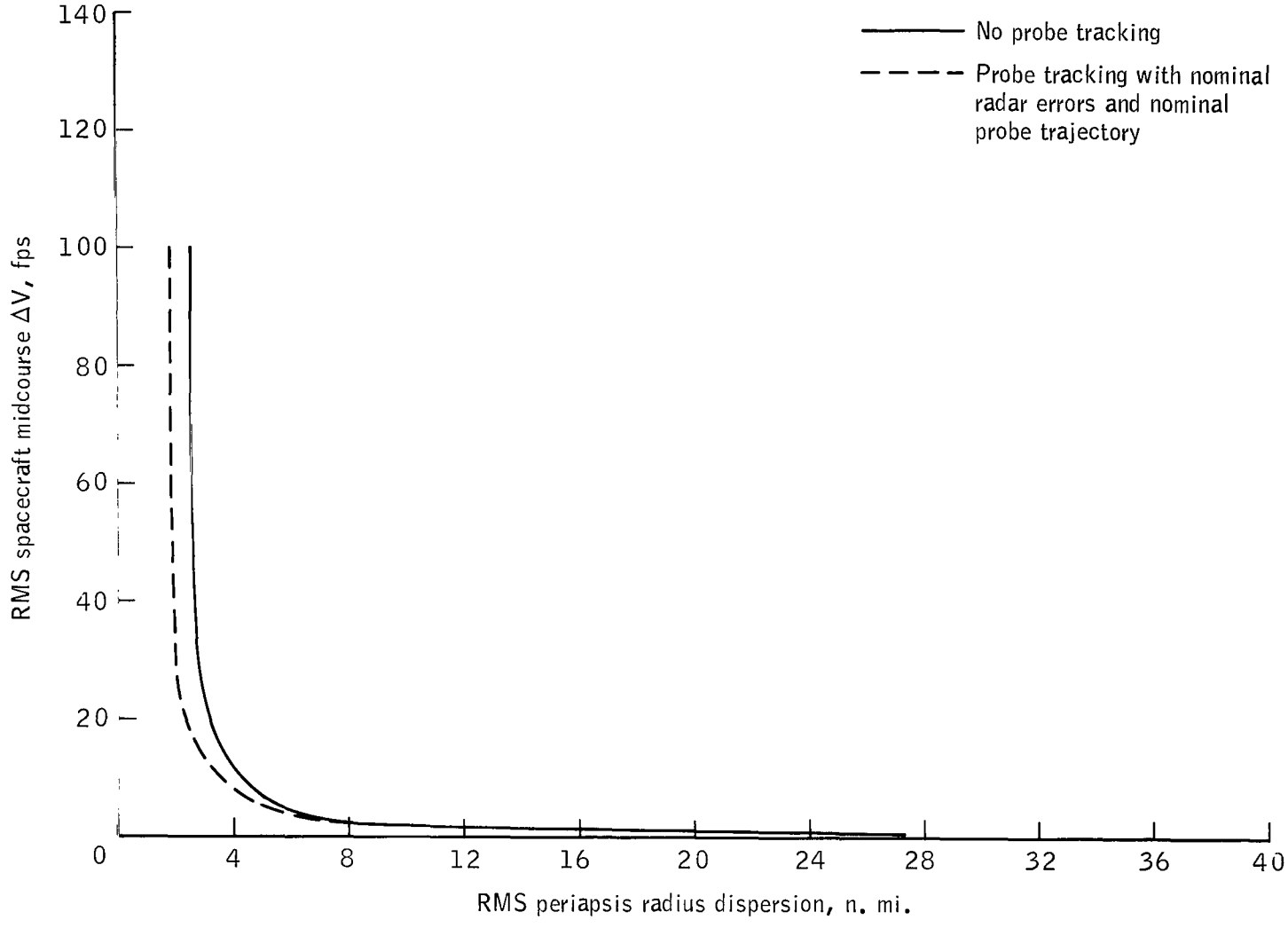

(b) Guidance error.

Figure 8. - Concluded.

NATIONAL AERONAUTICS AND SPACE ADMINISTRATION
WASHINGTON, D. C. 20546

OFFICIAL BUSINESS

FIRST CLASS MAIL

POSTAGE AND FEES PAID
NATIONAL AERONAUTICS AND
SPACE ADMINISTRATION

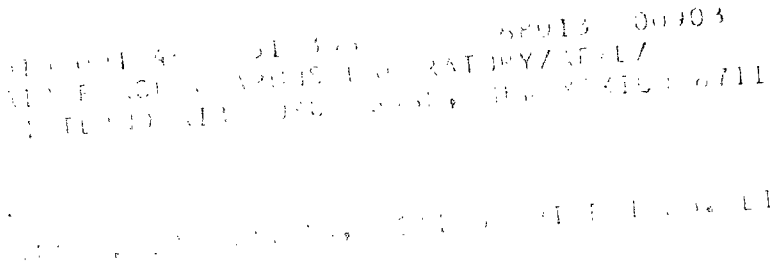

POSTMASTER: If Undeliverable (Section 158 Postal Manual) Do Not Return

"The aeronautical and space activities of the United States shall be conducted so as to contribute . . . to the expansion of human knowledge of phenomena in the atmosphere and space. The Administration shall provide for the widest practicable and appropriate dissemination of information concerning its activities and the results thereof."

—NATIONAL AERONAUTICS AND SPACE ACT OF 1958

NASA SCIENTIFIC AND TECHNICAL PUBLICATIONS

TECHNICAL REPORTS: Scientific and technical information considered important, complete, and a lasting contribution to existing knowledge.

TECHNICAL NOTES: Information less broad in scope but nevertheless of importance as a contribution to existing knowledge.

TECHNICAL MEMORANDUMS: Information receiving limited distribution because of preliminary data, security classification, or other reasons.

CONTRACTOR REPORTS: Scientific and technical information generated under a NASA contract or grant and considered an important contribution to existing knowledge.

TECHNICAL TRANSLATIONS: Information published in a foreign language considered to merit NASA distribution in English.

SPECIAL PUBLICATIONS: Information derived from or of value to NASA activities. Publications include conference proceedings, monographs, data compilations, handbooks, sourcebooks, and special bibliographies.

TECHNOLOGY UTILIZATION PUBLICATIONS: Information on technology used by NASA that may be of particular interest in commercial and other non-aerospace applications. Publications include Tech Briefs, Technology Utilization Reports and Notes, and Technology Surveys.

Details on the availability of these publications may be obtained from:

SCIENTIFIC AND TECHNICAL INFORMATION DIVISION

NATIONAL AERONAUTICS AND SPACE ADMINISTRATION

Washington, D.C. 20546